Electronic supplementary materials

For https://doi.org/10.1631/jzus.A2500531

Load characteristics and dynamic stability of hydrogen aerostatic gas bearings in turbo-expanders

Chenjie GU[1,2], Songqiang ZHU[1], Zhenyu LIU[2], Limin QIU[3], Yutao LIU[1], Kai FANG[1], Jingfeng LI[1]

[1]*Zhejiang Baima Lake Laboratory Co. Ltd., Hangzhou 310051, China*
[2]*School of Mechanical Engineering, Zhejiang University, Hangzhou 310058, China*
[3]*Institute of Refrigeration and Cryogenics, Zhejiang University, Hangzhou 310027, China*

S1 Mesh scheme and mesh independence

The mesh details of the flow field domain are illustrated in Fig. S1. Mesh refinement is performed in the orifice and gas film clearance regions to ensure the capture of intense flow variations within these areas.

The number of mesh layers in the gas film clearance significantly affects the accuracy of the simulation, as the thickness of this region is only 20 μm, and sharp variations in velocity and pressure occur along the film thickness. The results of meshes with 3, 5, 7, and 9 layers along the film direction were compared, and the total number of mesh elements corresponding to each case is 676,131, 1,059,631, 1,443,131, and 1,826,631, respectively. The inlet pressure is 0.6 MPa and the outlet pressure is 0.1 MPa in the simulations. Load capacity was calculated at rotational speeds of 0 rpm and 60,000 rpm respectively to verify mesh independence. The results are presented in Fig. S2. The load capacities at rotational speeds of 0 rpm and 60,000 rpm remain nearly unchanged when the number of layers increases from 7 to 9, with deviations of 0.87% and 0.99% respectively.

Therefore, cases of 7 layers in the film region are adopted to calculate the static and dynamic load capacities, considering both accuracy and computational time.

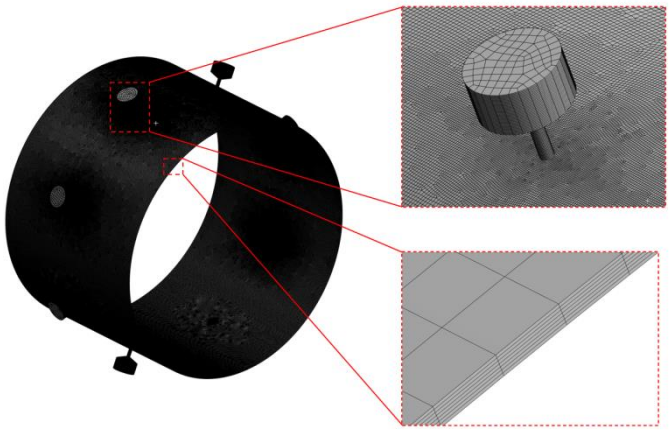

Fig. S1 Meshing of the gas film flow field

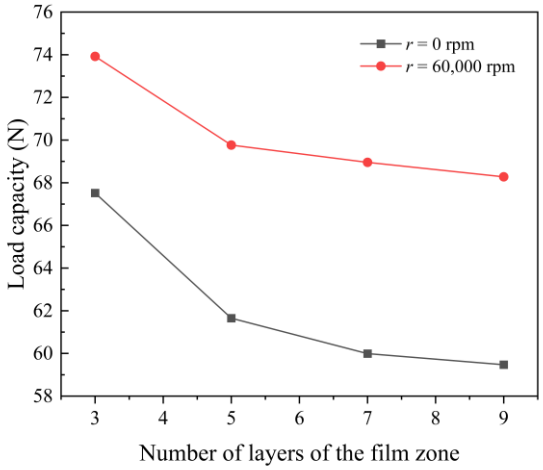

Fig. S2 Mesh independence verification of the model

S2 Pressure distribution

The circumferential and axial pressure distribution curves of the HAGB were extracted, which were compared with those of helium bearing exhibiting significant hydrodynamic effect, as shown in Fig. S3. The extraction was performed under eccentricity ratio of 0.6 and rotational speed of 60,000 rpm. It can be observed that the pressures of hydrogen and helium bearings at the orifices are basically consistent. However, under high rotational speeds, the pressures of the helium bearing at all positions are higher than those of the HAGB, and the pressure distribution in the high-pressure regions is more stable.

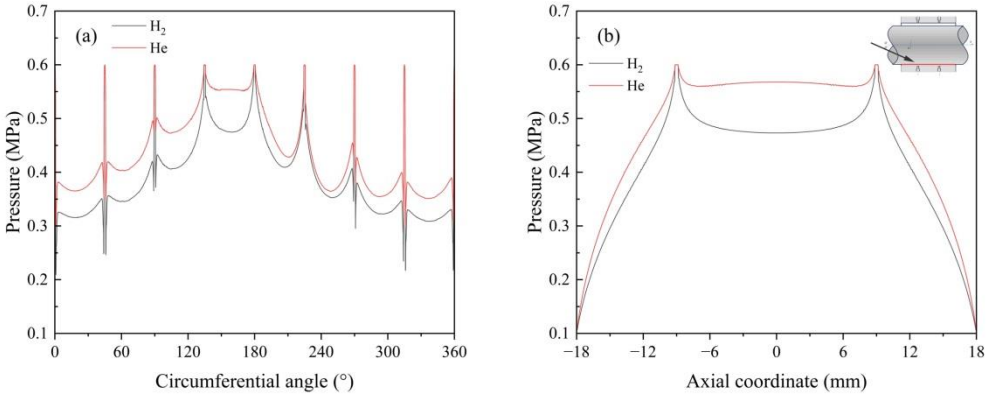

Fig. S3 Pressure distribution of gas bearings with hydrogen and helium: (a) axial pressure distribution; (b) circumferential pressure distribution

S3 Dynamic parameters

S3.1 Calculation method

The characteristics of hydrogen, like low density and low viscosity, make the dynamic parameters of the hydrogen gas film particularly important under external excitation. In this study,

the dynamic parameters are solved based on the pressure response of the rotor-bearing system to harmonic excitation, and the effects of operating and structural parameters on the dynamic characteristics of the HAGB are analyzed. The vibration equation is given as follows. The nonlinear gas film force can be linearized, assuming that the rotor undergoes only small disturbances around its equilibrium position.

$$\begin{bmatrix} K_{xx} & K_{xy} \\ K_{yx} & K_{yy} \end{bmatrix} \begin{pmatrix} x(t) \\ y(t) \end{pmatrix} + \begin{bmatrix} C_{xx} & C_{xy} \\ C_{yx} & C_{yy} \end{bmatrix} \begin{pmatrix} \dot{x}(t) \\ \dot{y}(t) \end{pmatrix} = \begin{pmatrix} F_x \\ F_y \end{pmatrix} \tag{S1}$$

where K_{ij} is the dynamic stiffness coefficient, which characterizes the force change in the i-direction caused by the displacement change in the j-direction. C_{ij} is the dynamic damping coefficient, which characterizes the velocity change in the i-direction caused by the displacement change in the j-direction. $x(t)$ and $y(t)$ are the displacement functions of the rotor in the x- and y-directions, respectively. $\dot{x}(t)$ and $\dot{y}(t)$ are the velocity functions of the rotor in the x- and y-directions, respectively.

It is assumed that the rotor is only subjected to a small harmonic disturbance in the y-direction, under which only harmonic vibration of the rotor in the y-direction will appear. The dynamic mesh method is applied to realize the harmonic disturbance of the rotor wall, which in turn characterizes the periodic deformation of the gas film. The harmonic disturbance in the y-direction is expressed as follows:

$$y(t) = Y_1 \sin(2\pi n f t + \varphi_1) \tag{S2}$$

where Y_1 is the amplitude of disturbance, f is the frequency corresponding to the rotational speed, and $\varphi_1$is the initial phase. n is the dimensionless disturbance frequency, which is the ratio of the disturbance frequency υ to the rotational speed frequency f, i.e., $n = \upsilon/f$.

The displacement and velocity components in the x-direction are 0, since the harmonic disturbance occurs only in the y-direction. Thus, the vibration equation can be rewritten as follows:

$$K_{xy} y(t) + C_{xy} \dot{y}(t) = -F_x(t) \tag{S3}$$

$$K_{yy} y(t) + C_{yy} \dot{y}(t) = -F_y(t) \tag{S4}$$

Similarly, when the rotor is only subjected to harmonic disturbance in the x-direction, the displacement and vibration equations in the x-direction are expressed as follows:

$$x(t) = X_1 \sin(2\pi n f t + \varphi_2) \tag{S5}$$

$$K_{xx} x(t) + C_{xx} \dot{x}(t) = -F_x(t) \tag{S6}$$

$$K_{yx} x(t) + C_{yx} \dot{x}(t) = -F_y(t) \tag{S7}$$

The 8 dynamic parameters under the corresponding conditions can be obtained by performing least-squares fitting to the vibration equation sets in the y-direction and x-direction, respectively.

S3.2 Effects of operational parameters

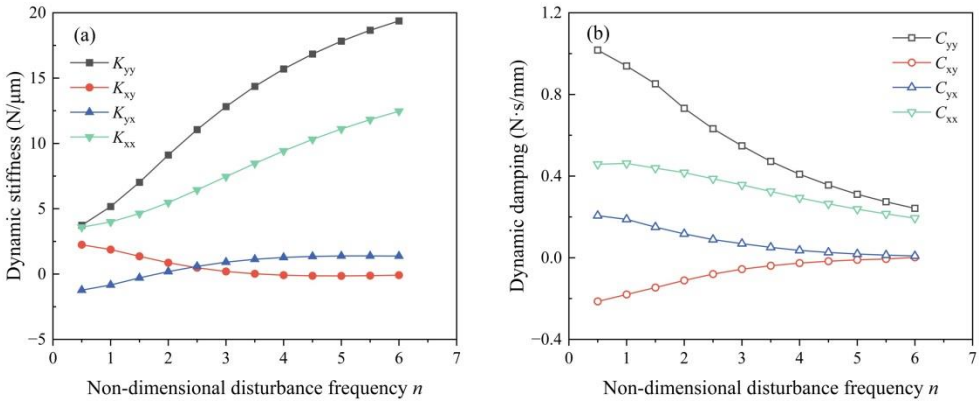

Fig. S4 Variation of dynamic characteristics of the HAGB with disturbance frequency: (a) dynamic stiffness; (b) dynamic damping

The variation of the dynamic stiffness and dynamic damping of the HAGB with the dimensionless disturbance frequency n is presented in Fig. S4. The direct stiffness coefficients characterize the radial support stiffness and centering capability of the gas bearing. The direct stiffness coefficients K_{yy} and K_{xx} increase with n, which increase by 418.5% and 247.5% from 0.5 to 6 respectively. The direct damping coefficients reflect the energy dissipation and vibration suppression effect of the gas film on rotor motion. The direct damping coefficients C_{yy} and C_{xx} decrease with n, with a decrease of 76.2% and 57.6% respectively. This indicates that the ability of the HAGB to resist vibrations under high-frequency disturbances will weaken. The cross-coupled stiffness coefficients represent the induced elastic forces in the transverse direction due to displacement in the orthogonal direction, which are the primary source of rotor whirling instability. While the cross-coupled damping coefficients describe the additional damping forces generated in the transverse direction by the velocity in the orthogonal direction, reflecting the energy dissipation effect of the gas film on rotor motion. Large positive cross-coupled stiffness coefficients can make the rotor prone to whirl, and the cross-coupled damping coefficients play a weakly stabilizing role in aerostatic gas bearings. The cross-coupled stiffness (K_{yx} and K_{xy}) and cross-coupled damping (C_{yx} and C_{xy}) tend toward 0 as n increases. The variation trends of all 8 dynamic parameters gradually flatten out with the increase of n.

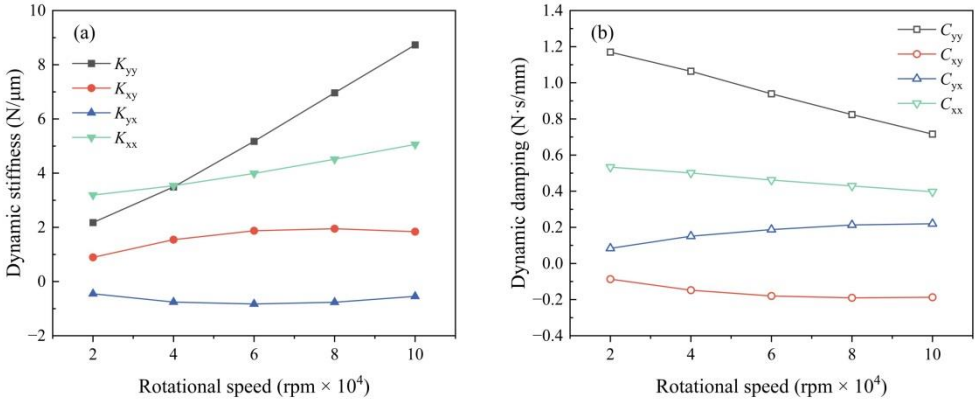

Fig. S5 Variation of dynamic characteristics of the HAGB with rotational speed: (a) dynamic stiffness; (b) dynamic damping

Since the unbalanced force acting on the rotor during rotation is mainly caused by its own eccentric mass, this unbalanced force primarily affects the dynamic stability at the rotational frequency. Therefore, the dynamic parameters of the HAGB were analyzed based on the rotational frequency corresponding to each rotational speed. The variation of the dynamic parameters with the rotational speed is presented in Fig. S5. The direct stiffness coefficients K_{yy} and K_{xx} increase by 301.1% and 58.5% respectively as the rotational speed rises from 20,000 rpm to 100,000 rpm. As the rotational speed increases, the flow Mach number in the hydrogen gas film rises and the compressibility effect of the gas is significantly enhanced, resulting in the lag of pressure fluctuation and the decrease in disturbance transfer efficiency. Consequently, the main damping coefficients C_{yy} and C_{xx} decrease by 38.8% and 25.5% respectively. The cross-coupled stiffness coefficients and cross-coupled damping coefficients exhibit little variation with the rotational speed. In bearings dominated by hydrostatic effects, the gas film pressure is mainly established by external pressurized gas supply rather than hydrodynamic shear effects, so these cross-coupled dynamic coefficients are relatively insensitive to changes in operating parameters.

The variation of the dynamic parameters with the supply pressure is presented in Fig. S6. As the supply pressure increases from 0.2 MPa to 1.0 MPa, K_{yy} and K_{xx} increase by 45.1% and 420.9% respectively. The increase in the supply pressure enhances the hydrostatic effect of the HAGB. A higher supply pressure raises the mean pressure within the gas film and enables a faster response to pressure fluctuations induced by small rotor displacements, thereby leading to an increase in direct damping. C_{yy} and C_{xx} increase by 119.6% and 66.8%, respectively. The cross-coupled stiffness coefficients and cross-coupled damping coefficients also exhibit little variation with the supply pressure.

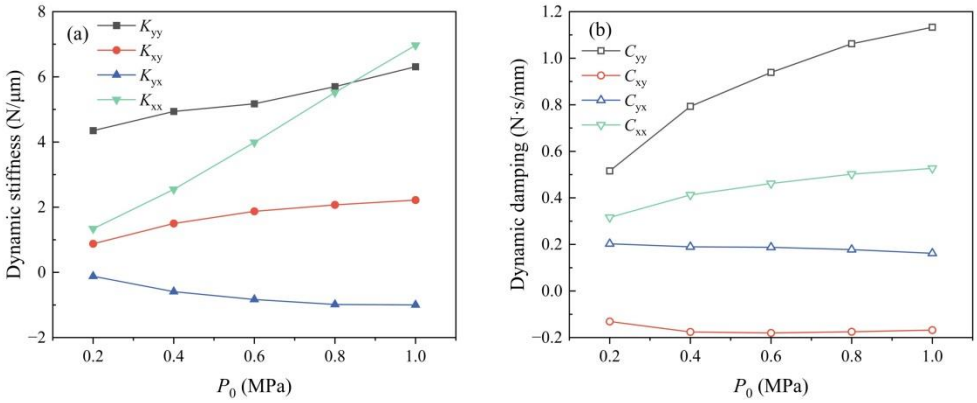

Fig. S6 Variation of dynamic characteristics of the HAGB with inlet pressure: (a) dynamic stiffness; (b) dynamic damping

S3.3 Effects of structural parameters

The variations in dynamic parameters of the HAGB caused by changes in the orifice diameter

are given in Fig. S7. As the orifice diameter increases from 0.15 mm to 0.35 mm, the direct stiffness coefficients K_{yy} and K_{xx} decrease by 16.1% and 22.6% respectively, indicating that the load capacity of the HAGB is weakened as the orifice diameter increases. The cross-coupled stiffness coefficient K_{yx} is negative throughout the calculation range, with its magnitude increased by 135.9%, and the K_{xy} increases by 37.4% within the calculation range. The orifice merely acts as a gas supply inlet and has limited influence on the pressure propagation and dynamic dissipation characteristics inside the gas film. Consequently, the dynamic damping coefficient shown in Fig. S7(b) exhibits an insignificant variation with the inlet orifice diameter.

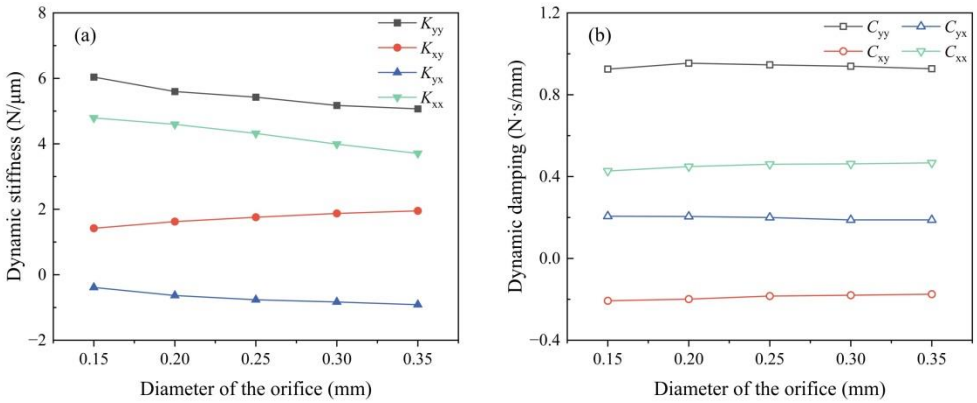

Fig. S7 Variation of dynamic characteristics of the HAGB with orifice diameter: (a) dynamic stiffness; (b) dynamic damping

The variation of the dynamic parameters with the gas film clearance is significant, as shown in Fig. S8. When the gas film clearance decreases to 10 μm, the hydrodynamic effect of the HAGB is improved, thus leading to the optimization of the direct stiffness coefficients and direct damping coefficients. As the gas film clearance increases from 10 μm to 30 μm, K_{yy} and K_{xx} decrease by 93.7% and 77.3% respectively, while C_{yy} and C_{xx} decrease by 88.5% and 92.5% respectively. The cross-coupled stiffness coefficients nearly do not change with the gas film clearance. When the gas film clearance is less than 25 μm, the optimization effect on the dynamic parameters is significant. While when it exceeds 25 μm, the dynamic parameters tend to stabilize.

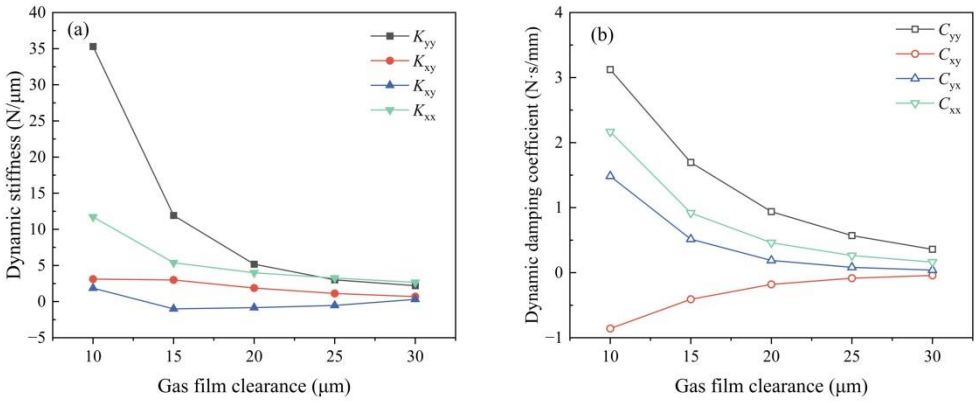

Fig. S8 Variation of dynamic characteristics of the HAGB with gas film clearance: (a) dynamic stiffness; (b) dynamic damping